Scripta Materialia 152 (2018) 24–26

Contents lists available at ScienceDirect

Scripta Materialia

journal homepage: www.elsevier.com/locate/scriptamat

Regular article

First measurement of the full elastic constants of Ni-based superalloy René 88DT

Xinpeng Du, Ji-Cheng Zhao *

Department of Materials Science and Engineering, The Ohio State University, 2041 College Road, Columbus, OH 43210, USA

ARTICLE INFO

Article history:
Received 8 March 2018
Received in revised form 28 March 2018
Accepted 31 March 2018
Available online xxxx

Keywords:
Elastic constants
Laser ultrasonics
Superalloy René 88DT
Young's modulus
Mechanical testing

ABSTRACT

The full elastic constants of Ni-based superalloy René 88DT were measured for the first time using a recently developed method that matches the computed surface acoustic wave (SAW) velocities from an elastodynamic model with experimental velocities of SAWs that are generated and detected with a femtosecond laser. The experimental measurements were performed on several grains of a polycrystalline sample without the need of growing a single crystal. The computed Young's modulus from the resultant elastic constants agrees with the literature values, lending confidence on our measured elastic constants: $C_{11} = 267.1$, $C_{12} = 170.5$, and $C_{44} = 107.6$ (GPa).

René 88DT is one of the powder metallurgy superalloys [1,2]; and it is one of the most widely used ones for jet engine high pressure turbine disks. Its composition is Ni-16Cr-13Co-4Nb-4W-2.1Al-3.7Ti-0.7Nb-0.03C-0.015B (wt%, Ni-balance). René 88DT has an excellent combination of tensile and creep strength as well as corrosion and oxidation resistance at elevated temperatures [3]. Various studies have been performed over the years on its phase structures [4] and the effect of constituent elements [5], creep deformation mechanisms at elevated temperatures [6,7], and fatigue crack initiation mechanisms under cyclic loading [8–10].

The elastic behavior of René 88DT is much less studied and its full elastic constants have never been reported yet, most likely due to the fact it is a significant undertaking to grow a single crystal out of such a complex powder metallurgy composition for elastic constant measurement. Nevertheless, extensive studies on the fatigue initiation mechanism of René 88DT show that elastic anisotropy plays a significant role on the crack initiation process [8–10]. Moreover, elastic constants are essential parameters for various micro-mechanics models, such as fatigue sensitivity [11], failure mechanism at microscale [12], crack nucleation mechanisms [13], fatigue-crack-initiation interaction [14] and so on. Thus, accurate elastic constant values of René 88DT will significantly help improve the accuracy of these models.

Traditional tensile stress-strain measurement has been used to evaluate the Young's modulus of René 88DT [15]. The DIC (Digital Image Correlation) technique afforded measurement of local strains of polycrystals in both elastic and plastic regimes to help measure Young's modulus more accurately [16–18]. Hardness test has been used to measure the mechanical strength of Nickel-based superalloys [19]. These methods, however, can only result in an average measurement of Young's modulus rather than the full elastic constants.

Recently, Du and Zhao have developed a new method that enables measurement of the full elastic constants from polycrystalline samples by integrating experimental measurement of femtosecond laser induced SAWs with high precision elastodynamic modeling [20]. The model based on elastic dynamics was established as follows to allow computation of SAW and other bulk and surface modes along any crystal orientation of any crystal structure when the elastic constants and density are given:

$$C_{ijkl}\frac{\partial^2 U_l}{\partial x_j \partial x_k} = \rho\frac{\partial^2 U_i}{\partial t^2} \qquad x_3 \le 0 \tag{1}$$

$$\sigma_{i3}|_{z=0} = C_{i3kl}\frac{\partial U_l}{\partial x_k}|_{z=0} = \delta_{i3}\delta(x,y)\delta(t) \tag{2}$$

$$U_i(x,y,z,t) = 0, \quad \text{when } x,y,z,t \to \infty \tag{3}$$

$$U_i(x,y,z,t) = 0 \quad \text{for } t < 0 \tag{4}$$

where, C_{ijkl} represents the elastic constants, U_i the displacement, ρ the density, σ_{ij} the stress, x the space, t the time, respectively. Subscript i,j, k,l are all from 1 to 3. The Dirac delta function and Einstein summation convention are both applied. By applying triple Fourier transform on the

* Corresponding author.
E-mail address: zhao.199@osu.edu. (J.-C. Zhao).

https://doi.org/10.1016/j.scriptamat.2018.03.044
1359-6462/

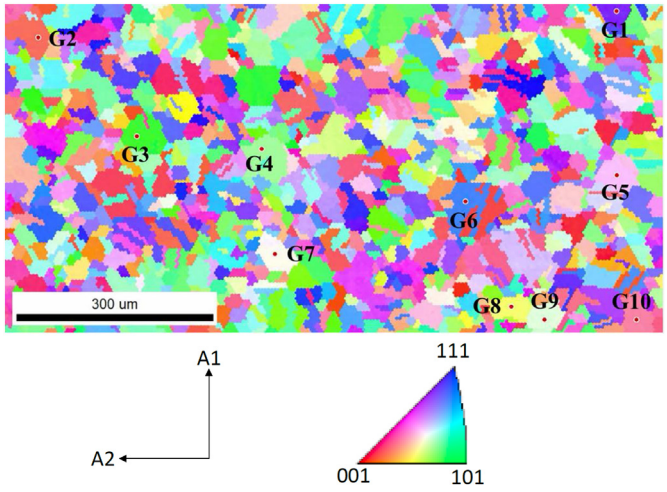

Fig. 1. EBSD inverse pole figure of (001) with the reference frame and orientation map shown. The scanning region was 1000 μm × 500 μm with a step size of 5 μm in both directions. Based on the grain size and distribution, 10 grains were selected and labeled for SAW measurements.

temporal variable and the two spatial variables parallel to the surface of the semi-infinite system, the differential equation was solved. As a result, the SAW velocities could be expressed as a function of elastic constants, orientation and density [20,21].

Our method combines experiments generating and detecting SAW velocities along various orientations with models predicting SAW velocities along the same orientations. A forward optimization algorithm was used to iteratively match experimental measurements with model calculations to eventually extract the full elastic constants. This method enables us to measure the full elastic constants of René 88DT without making single crystals.

A bulk piece of René 88DT was provided by GE Global Research and a small piece of the sample was cut with a diamond saw and then placed in an air furnace for heat treatment at 1150 °C for 50 h. The oxidation resistance of René 88DT is so good that a protective oxide scale was formed to protect the sample from internal oxidation. The center of the sample was unaffected by any oxidation effect. As 1150 °C was higher than the solvus line (roughly 1105 °C) of the gamma prime phase, no gamma prime precipitate would expect to form at 1150 °C. This heat treatment served the dual purpose of both growing the grain size and forming the fcc solid solution phase to reduce the potential interference of the gamma prime phase during the measurements. After the heat treatment, the sample was directly taken out of the furnace and cooled down to ambient temperature. It was mounted in regular metallographic bakelite, grinded with SiC sand papers of 120, 320, 600, 800, 1200 grit sizes in sequence in water, and polished with a vibratory polishing machine in 0.05 μm colloidal silica suspension for 48 h to obtain a high quality surface finish.

Microhardness indents were placed on the sample surface to denote a region (1000 μm × 500 μm) of interest. Electron backscattering diffraction (EBSD) characterization was carried out on a XL-30 ESEM system (FEI, Inc.) with a high-brightness field-emission electron gun. The acceleration voltage was 20 kV. The working distance was 20 mm. The step size was 5 μm in each direction. The collected data was then analyzed on a TSL software platform. The collected inverse pole figure of (001) showing in Fig. 1 displays the distribution of the grain size and orientation.

Ten large grains with distinct orientations were selected for the SAW experiment. Before performing laser experiments, a parallel-grating organic film made of polydimethylsiloxane (PDMS) was prepared to cover the entire region. This film is used to assist the acquisition of narrow-band SAW waves that only survived along one direction (perpendicular to the PDMS grating lines) in SAW experiments. The PDMS films were made by mixing Sylgard 184 silicone elastomer base and its curing agent at a ratio of ten to one. Then it was cured in a 1D grating Si mold at 80 °C for several days. After curing, a PDMS film with 700 nm periodicity, 50% duty cycle and a groove depth 350 nm was obtained. More details about the fabrication and use of the PDMS film can be found elsewhere [22].

Our SAW experiment was based on time-domain thermoreflectance (TDTR) [20,22,23] which employs a laser beam to inject heat into the surface of a sample and a second laser beam to probe surface temperature as a function of time through temperature dependence of the optical index of refraction. A mode-locked Ti:sapphire laser was employed in a pump-probe two-beam configuration. The pump beam was used to generate SAWs on the sample surface and the probe beam was employed to detect the SAWs generated by the pump beam. Both beams coincided at the same position on the sample surface but arrived at different times through the use of a computer-controlled optical delay stage. By detecting the SAW profile as a function of the time delay between the pump and probe beams, the SAW velocity could be obtained [20,22], as shown in Fig. 2 as an example.

SAW measurements were conducted on 10 grains as labeled in Fig. 1 under two different PDMS orientations. In other words, we performed one set of measurements and then rotated the PDMS film orientation and performed a second set of measurements. For each grain, four points around the grain center were measured to get SAW velocities. The results of one SAW measurement on Grain 10 under PDMS orientation 1 are shown in Fig. 2 to demonstrate the data in both time domain

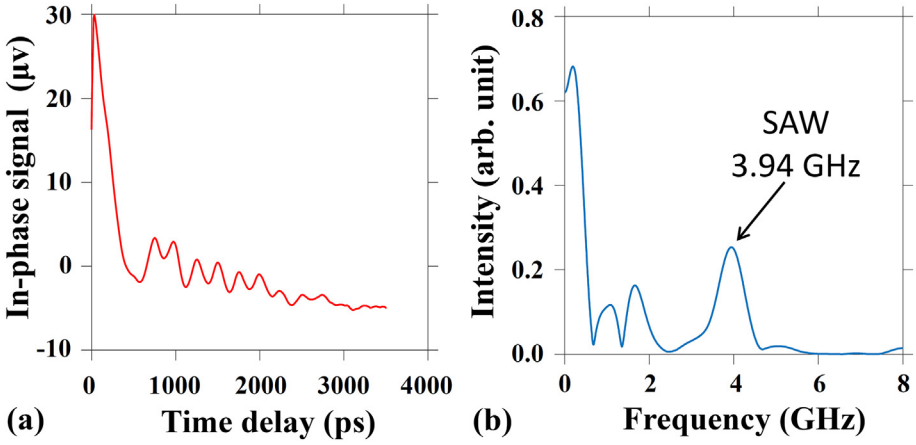

Fig. 2. (a) Time domain signal of a SAW wave obtained by detecting the SAW profile as a function of the delay time between the pump and the probe beam; (b) Frequency domain signal of the SAW wave obtained by performing a Fourier transform on the time domain signal. The SAW peak could be identified in the frequency domain signal, and the SAW velocity is equal to the frequency times the wavelength which is 700 nm that is dictated by the PDMS film grating.

Table 1
Comparison of the experimental ($V_{expt.}$) and computed (V_{model}) SAW velocities.

Grain	Euler angles (degree)	PDMS orientation (degree)	$V_{expt.}$ (m/s)	V_{model} (m/s)	Difference (%)
G5	[95.1, 76.2, 26.8]	89.6	2495.5	2451.0	−1.78
G6	[348.7, 64.4, 43.0]	89.6	2473.7	2606.1	5.35
G7	[34.8, 79.2, 241.0]	89.6	2496.7	2588.8	3.69
G8	[225.1, 93.0, 154.8]	89.6	2869.3	2867.7	−0.06
G9	[209.0, 32.8, 160.6]	89.6	2507.7	2509.0	0.05
G10	[136.9, 19.9, 297.6]	89.6	2756.5	2690.2	−2.41
G1	[215.4, 118.5, 145.6]	60.1	2648.5	2690.2	1.57
G2	[203.0, 86.3, 169.5]	60.1	2638.8	2501.8	−5.19
G3	[13.6, 88.5, 47.0]	60.1	2575.6	2581.1	0.21
G4	[26.8, 35.6, 102.4]	60.1	2517.4	2649.5	5.25
G5	[95.1, 76.2, 26.8]	60.1	2619.3	2617.8	−0.06
G7	[34.8, 79.2, 241.0]	60.1	2573.2	2569.8	−0.13
G8	[225.1, 93.0, 154.8]	60.1	2756.5	2552.9	−7.39
G9	[209.0, 32.8, 160.6]	60.1	2625.0	2482.3	−5.44
G10	[136.9, 19.9, 297.6]	60.1	2718.8	2571.6	−5.41

and frequency domain to explain how the SAW velocity was evaluated. The velocities reported in Table 1 are the average velocity of four measurements on each grain under each orientation. The laser spot size of this experiment was ~5 μm, enabling high spatial resolution of the measurements since the SAW attenuates quickly beyond the laser spot by the PDMS film.

To obtain the direction associated with the measured velocity, Euler angles measured using EBSD and the PDMS film orientation measured by light microscope were both employed. Some measurements were not included in the analysis due to either small signal-to-noise ratios or wide variability of the velocities within a grain. The results of the reliable measurements were summarized in Table 1 with a total of 15 experimental SAW velocities, which spanned a range of ~2500 m/s to ~2870 m/s, indicating high anisotropy of René 88DT. Those experimental velocities were to be matched by the computed SAW velocities from the elastodynamic model with elastic constants, density and orientation as input parameters. Our forward optimization method was based on Nelder-Mead simplex method. At any given initial value of elastic constants, the method would begin to update the elastic constants iteratively, aimed at minimizing the difference between calculated SAW velocities and experimental SAW velocities. As it only converges to a local optimum, multiple initial values were provided to achieve the best fit possible.

A total of 45 initial values were equally sampled for C_{11}, C_{12} and C_{44} and put into the forward optimization algorithm. The best fit yields the elastic constants as $C_{11} = 267.1$ GPa, $C_{12} = 170.5$ GPa, and $C_{44} = 107.6$ GPa. The anisotropic ratio is 2.23, which is quite high. The computed and measured SAW velocities are in excellent agreement as shown in Table 1. The density of René 88DT used in the computation is 8.36 g/cm^3 [24]. Since there are no literature elastic constants for a direct comparison with our results, the elastic constants are used to compute the aggregate polycrystalline properties such as Young's modulus and Poisson's ratio for comparison. The computed/aggregated Young's modulus from our elastic constants is between 194 and 221 GPa (the lower and upper bonds) using the widely employed Voigt and Reuss averaging schemes [25], which agrees well with the literature Young's modulus values ranging from 210 to 220 GPa that were obtained from bulk sample measurements [5,26]. The aggregated Poisson's ratio computed from our elastic constants is between 0.32 and 0.34.

The current measurement was made at ambient temperature. The PDMS film may still be workable for temperatures up to 200 °C above which a different grating film or an alternative grating scheme need to be identified or developed. To prevent sample surface oxidation at higher temperatures (e.g., >400 °C), the sample needs to be put inside a vacuum with an optical window to allow laser beam access. Such measurements at the working temperatures of the alloy are highly desired and will be pursued in the future.

In summary, a new SAW-PDMS-TDTR-MODEL method was applied to measure the full elastic constants of René 88DT from a polycrystalline sample. SAW velocities along 15 distinct orientations were experimentally measured and were fitted with a robust elastodynamic model through a forward optimization algorithm. The full elastic constants of René 88DT were obtained and reported for the first time as $C_{11} = 267.1$ GPa, $C_{12} = 170.5$ GPa, and $C_{44} = 107.6$ GPa. This new method can be employed to measure elastic constants of any polycrystalline sample with a grain size larger than 30 μm as demonstrated in this study, thus it will greatly facilitate future measurements of elastic constants for complex alloys without the need of growing single crystals.

Acknowledgment

This study was funded under U.S. National Science Foundation (NSF) under grant number 1237577. The authors are grateful to GE for providing the René 88DT sample that was used for our measurement.

References

[1] E.S. Huron, P.G. Roth, Superalloys 1996, 1996 359–368.
[2] G. Raisson, Powder Metall. 51 (2008) 10–13.
[3] R. Schafrik, R. Sprague, Adv. Mater. Process. 162 (2004) 29–33.
[4] S. Wlodek, M. Kelly, D. Alden, Superalloys 1996, 1996 129–136.
[5] T.M. Pollock, S. Tin, J. Propuls. Power 22 (2006) 361–374.
[6] R.R. Unocic, G.B. Viswanathan, P.M. Sarosi, S. Karthikeyan, J. Li, M.J. Mills, Mater. Sci. Eng. A 483–484 (2008) 25–32.
[7] G.B. Viswanathan, S. Karthikeyan, P.M. Sarosi, R.R. Unocic, M.J. Mills, Philos. Mag. 86 (2006) 4823–4840.
[8] J. Miao, T.M. Pollock, J.W. Jones, Superalloys 2008, 2008 589–597.
[9] J.C. Stinville, W.C. Lenthe, J. Miao, T.M. Pollock, Acta Mater. 103 (2016) 461–473.
[10] J. Miao, T.M. Pollock, J.W. Jones, Acta Mater. 57 (2009) 5964–5974.
[11] M. Shenoy, J. Zhang, D.L. McDowell, Fatigue Fract. Eng. Mater. Struct. 30 (2007) 889–904.
[12] A. Cerrone, J. Tucker, C. Stein, A. Rollett, A. Ingraffea, 2012 Jt. Conf. Eng. Mech. Inst. 11th ASCE Jt. Spec. Conf. Probabilistic Mech. Struct. Reliab, 2012 1–10.
[13] K.O. Findley, A. Saxena, Metall. Mater. Trans. A 37 (2006) 1469–1475.
[14] K.S. Chan, Metall. Mater. Trans. A 34A (2003) 43–58.
[15] M.J. Caton, S.K. Jha, A.H. Rosenberger, J.M. Larsen, Superalloys 2004, 2004 305–312.
[16] J.C. Stinville, M.P. Echlin, D. Texier, F. Bridier, P. Bocher, T.M. Pollock, Exp. Mech. 56 (2016) 197–216.
[17] M.A. Tschopp, B.B. Bartha, W.J. Porter, P.T. Murray, S.B. Fairchild, Metall. Mater. Trans. A 40A (2009) 2363–2368.
[18] J.C. Stinville, N. Vanderesse, F. Bridier, P. Bocher, T.M. Pollock, Acta Mater. 98 (2015) 29–42.
[19] H. Wu, J. Li, F. Liu, L. Huang, X. Zeng, Q. Fang, Z. Huang, L. Jiang, Mater. Des. 128 (2017) 176–181.
[20] X. Du, J. Zhao, npj Comput. Mater. 3 (2017) 17.
[21] P. Zhao, J.-C. Zhao, R. Weaver, J. Acoust. Soc. Am. 133 (2013) 2634–2640.
[22] D. Li, P. Zhao, J.-C. Zhao, D.G. Cahill, J. Appl. Phys. 114 (2013) 143102.
[23] D.G. Cahill, Rev. Sci. Instrum. 75 (2004) 5119–5122.
[24] D.D. Krueger, R.D. Kissinger, R.G. Menzies, Superalloys 1992, 1992 277–286.
[25] R. Hill, Proc. Phys. Soc. A 65 (1952) 349–354.
[26] M. Tufft, The 7th Inter. Conf. on Shot Peening (ICSP7), 1999 254–263https://www.shotpeener.com/library/detail.php?anc=1999036.